COMPUTATIONAL STUDIES ON SOLAR PLASMA PHYSICS

HONG POU (ISABELLA) CHAN
The University of Edinburgh - The University of Tokyo

Supervised by PROF. TAKAAKI YOKOYAMA
Department of Earth and Planetary Science, The University of Tokyo

THE UNIVERSITY OF TOKYO RESEARCH INTERNSHIP PROGRAM (UTRIP)
28th June - 9th August 2016

ABSTRACT

Magnetohydrodynamic simulations were performed to extend the studies in spicule formation mechanism in the solar atmosphere. Based on Kudoh & Shibata (1999), the simulations were reproduced for a rigid wall boundary condition at the photosphere. The results show that Alfvén waves can be generated by random motions in the photosphere. As the Alfvén waves propagate upwards in the chromosphere, longitudinal slow and fast waves are excited through nonlinear couplings. These longitudinal motions then develop into shocks and eventually lift up the transition region as they propagate upwards in the solar atmosphere. The model was then modified to include a convection zone underneath the photosphere by solving adiabatic energy equations. Simulations of the modified model reveal that the convection zone has an effect on the height of spicules. In order to generate spicules of the same height, the amount of input torque in the photosphere in the modified model is ~ 90 times larger than that of Kudoh & Shibata's model.

1. INTRODUCTION

Spicule is one of the most fundamental components of the higher solar atmosphere. Spicules are solar jets ejected from the surface of the Sun at supersonic speed along magnetic field lines, reaching a height of 5000-7000 km above the photosphere with a typical lifetime of ~5 minutes.

The formation mechanisms of spicules are still under debate. One of the promising ones is the non-linear interaction of the Alfvén wave generated at the photosphere (Hollweg et al. 1982; Hollweg 1992). Kudoh & Shibata (1999, hereafter KS99) examined this model by one-dimensional magnetohydrodynamic (MHD) simulations and considered the case in which Alfvén wave is excited by random perturbations instead, which results in the transition region being lifted up to more than ~ 5000 km, i.e. the spicule is produced.

In this UTRIP project, the formation mechanisms of solar spicules were studied. This research is motivated by the challenges arising from the limited observational data of solar spicules. Through numerical simulations, various developed theories of the spicule formation mechanism can be tested and studied. This project aims to test and extend the theory studied in KS99. This project studies the effects of boundary condition and implements a realistic model of the boundary between the convection zone and the photosphere by modifying the model from KS99. For this purpose, I learned magneto-hydrodynamics (MHD) and MHD waves (Section 2).

Section 2 will give an overview of magneto-hydrodynamics (MHD) and the properties of MHD waves. The basic equations, initial and boundary conditions, and numerical methods will be introduced in section 3. The spicule formation mechanism, Kudoh & Shibata's model and the modified model will also be described in detail. Section 4 will present some numerical simulations of both models and describe the properties of spicules. Results of the simulations will be analysed in section 5 and the conclusion is summarised in section 6.

2. MHD EQUATIONS AND MHD WAVES

Magnetohydrodynamics is a fluid theory which concerns the dynamics of magnetically confined plasma. The ideal MHD equations describe the motion of a perfectly conducting fluid, e.g. plasma, interacting with a magnetic

field. The interaction is described by combining Maxwell's equations with the equations of gas dynamics.

Maxwell's equations describe the evolution of the electric field ***E(r,t)*** and the magnetic field ***B(r,t)*** in response to the current density ***j(r,t)*** and the space charge ***r(r,t)***.

$$\nabla \times \mathbf{E} = -\frac{\partial \mathbf{B}}{\partial t} \quad (1)$$

$$\nabla \times \mathbf{B} = \mu_o \mathbf{j} + \frac{1}{c^2}\frac{\partial \mathbf{E}}{\partial t} \quad (2)$$

$$\nabla \cdot \mathbf{E} = \frac{r}{\epsilon_o} \quad (3)$$

$$\nabla \cdot \mathbf{B} = 0 \quad (4)$$

where c is the speed of light. Gas dynamics equations describe the evolution of the density ρ***(r,t)*** and the pressure ***p(r,t)***.

$$\frac{\mathrm{d}\rho}{\mathrm{d}t} + \rho \nabla \cdot \mathbf{v} \equiv \frac{\partial \rho}{\partial t} + \nabla \cdot (\rho \mathbf{v}) = 0 \quad (5)$$

$$\frac{\mathrm{d}p}{\mathrm{d}t} + \gamma p \nabla \cdot \mathbf{v} \equiv \frac{\partial p}{\partial t} + \mathbf{v} \cdot \nabla p + \gamma p \nabla \cdot \mathbf{v} = 0 \quad (6)$$

$$\rho \frac{\mathrm{d}\mathbf{v}}{\mathrm{d}t} = \mathbf{F} \equiv -\nabla p + \rho \mathbf{g} + \mathbf{j} \times \mathbf{B} + \tau \mathbf{E} \quad (7)$$

The interaction between variables ***E***, ***B,*** ρ and p is introduced through equation(7) involving the velocity ***v(r,t)*** of the fluid. Equation(7) expresses the acceleration of a fluid element (LHS) caused by the force **F** consisting of pressure gradient, gravity, and electromagnetic contributions (RHS).

For non-relativistic MHD motions, neglecting displacement current and space charge effects (since they are small), the basic equations of ideal MHD are obtained:

Continuity equation:

$$\frac{\partial \rho}{\partial t} + \nabla \cdot (\rho \mathbf{v}) = 0 \quad (8)$$

Momentum equation:

$$\rho \frac{\partial \mathbf{v}}{\partial t} + \rho \mathbf{v} \cdot \nabla \mathbf{v} + \nabla p - \mathbf{j} \times \mathbf{B} = \rho \mathbf{g}, \quad j = \frac{1}{\mu_0} \nabla \times \mathbf{B}, p = (\gamma - 1)\rho e \quad (9)$$

Internal energy equation:

$$\frac{\partial e}{\partial t} + \mathbf{v} \cdot \nabla e + (\gamma - 1) e \nabla \cdot \mathbf{v} = 0 \quad (10)$$

Induction equation:

$$\frac{\partial \mathbf{B}}{\partial t} + \nabla \times \mathbf{E} = 0, \quad \nabla \cdot \mathbf{B} = 0 \quad (11)$$

Solving the magnetohydrodynamic equations for small perturbations in a homogeneous background gives four solutions for four different wave modes propagating in the fluid, each at their own phase velocity along a magnetic field line. They are marginal entropy wave (with angular frequency, ω, = 0), in which there is only entropy (internal energy and density) perturbations; Alfvén waves (ω = ± ω_A, $\omega_A \equiv \mathbf{k} \cdot \mathbf{b}$ = kb cos θ, where **k** is the wave vector, **b** is the vectorial Alfvén speed and θ is the angle between **k** and **b**), in which there is perturbations in only velocity and magnetic field, thus incompressible and purely transverse; and fast and slow magneto-acoustic waves (ω = ± $\omega_{s,f}$,

$$w_{s,f} = \pm k \sqrt{0.5(b^2 + c_s^2) \pm 0.5\sqrt{(b^2 + c_s^2)^2 - 4(k_{//}^2/k^2) b^2 c_s^2}}$$

where the first ± sign refers to wave propagation to the right (+) and to the left (-), and the second ± sign refers to the fast (+) slow (-) magneto-acoustic wave, respectively), in which fast wave can propagate both perpendicular and parallel to magnetic field line ($\mathbf{B}_0$) but slow wave can only propagate parallel to $\mathbf{B}_0$.

3. THE NUMERICAL MODEL

This project extends Kudoh & Shibata's research and thus adopts many features from their numerical model. KS99 studied the generation of spicule by longitudinal shock waves. They produced magnetohydrodynamic simulations which show that random motions in the photosphere can generate Alfvén waves. As the Alfvén waves propagate upwards into the corona, longitudinal motions are excited by nonlinear coupling, which then develop into shock waves. The longitudinal shock waves propagate upwards and lift up the transition region, producing a spicule. Alfvén waves continue to propagate upward into the corona and contribute both to coronal heating and the non thermal broadening of emission lines.

KS99 used the same formulation that was used by Hollweg et al. (1982) and they both examine the Alfvén wave model. Hollweg et al. (1982) considered sinusoidal perturbation with a finite duration in the photosphere as the source for generating the Alfvén wave whereas

KS99 considered random perturbations in the photosphere throughout the calculation instead.

3.1 Basic Equations and Initial Conditions

The numerical model from KS99 is used in this project. Local curvilinear coordinate *(n, ϕ, s)* is used, where *s* is the distance measured along the poloidal field line, *n* is the distance perpendicular to the poloidal field line, and *ϕ* is the azimuthal angle measured around the rotation axis of the flux tube. This model uses the 1.5-dimensional approximation, i.e.,

$$\frac{\partial}{\partial \phi} = 0, \frac{\partial}{\partial n} = 0, v_n = 0, B_n = 0 \tag{12}$$

where v_n and B_n are the velocity and the magnetic field perpendicular to the poloidal magnetic field, respectively. Kudoh & Shibata assumed ideal MHD (inviscid, adiabatic, perfect conductor) in the flux tube. The basic equations are as follows: mass conservation,

$$\frac{\partial \rho}{\partial t} + v_s \frac{\partial \rho}{\partial s} = -\rho B_s \frac{\partial v_s}{\partial B_s}; \tag{13}$$

the *s* component of the momentum equation,

$$\frac{\partial v_s}{\partial t} + v_s \frac{\partial v_s}{\partial s} = -\frac{1}{\rho}\frac{\partial P}{\partial s} - g\frac{\partial z}{\partial s} + \frac{v_\phi^2}{r}\frac{\partial r}{\partial s} - \frac{1}{r\pi\rho}\frac{B_\phi}{r}\frac{\partial}{\partial s}(rB_\phi); \tag{14}$$

the *ϕ* component of the momentum equation,

$$\frac{\partial r v_\phi}{\partial t} + v_p \frac{\partial r v_\phi}{\partial s} = \frac{B_s}{r\pi\rho}\frac{\partial}{\partial s}(rB_\phi) + L(t,s), \tag{15}$$

the *ϕ* component of the induction equations,

$$\frac{\partial}{\partial t}\left(\frac{B_\phi}{rB_s}\right) + \frac{\partial}{\partial s}\left(\frac{B_\phi}{rB_s}v_s - \frac{v_\phi}{r}\right) = 0 \ ; \tag{16}$$

the adiabatic energy equation,

$$\frac{\partial e}{\partial t} + v_s \frac{\partial e}{\partial s} = -(\gamma - 1)eB_s \frac{\partial}{\partial s}\left(\frac{v_s}{B_s}\right); \tag{17}$$

and the equation of state, assumed to be that of ideal gas,

$$e = \frac{1}{\gamma - 1}\frac{P}{\rho}; \tag{18}$$

where *r* is the distance from the axis of the flux tube, which is assumed to be constant in this paper, ρ is the density, P is the thermal pressure, *e* is the specific internal energy, v_s is the velocity along the poloidal magnetic field, v_ϕ is the azimuthal velocity, B_s and B_ϕ are the poloidal and toroidal components of the magnetic field, respectively, g = 2.722 x 10^4 cm s^{-2}, is the gravitational acceleration, which is assumed to be constant, and the ratio of specific heats, γ, is assumed to be γ = 5/3. The function *L*(t,s) is the artificial torque, which is a source term for Alfvén waves in KS99.

While implementing KS99's model, we altered the geometry of the open magnetic flux tube from expanding within the chromosphere to being constant throughout the whole region. The shape of the flux tube from the photosphere is assumed to be fixed in the solar atmosphere, but torsional motion of the tube is allowed (1.5-dimensional approximation). See Figure 1 for the configuration of this magnetic field.

The pressure scale height, H_0, in the photosphere is taken to be 150 km. The time scale, t_0, which is calculated by dividing H_0 by the speed of sound in the photosphere (c_0 = 10 km s^{-1}), is 15 s in this paper. The radius of the field lines is taken to be $r_0 = H_0$. The ratio of magnetic pressure to gas pressure, plasma beta, β (=$8\pi P/B_s^2$), as a function of height is shown in Figure 2. In the photosphere, β is assumed to be 1. The gravity in the solar atmosphere (g = 2.84 x 10^4 cm s^{-2}) is set to be constant. The initial transition region height is taken to be ~ 15 H_0 = 2250 km. The temperature (T) as a function is shown in equation 19, which shows sudden increase at the transition region:

$$T/T_0 = 1 + 0.5(a_c - 1)\{1 + \tanh[(z - z_d)/0.5]\}, \tag{19}$$

where T_0 is the temperature in the photosphere and a_c is a parameter that determines the coronal temperature, which is 300 in this paper. The temperature in the photosphere is $T_0 = m_p g H_0/k \simeq 5000$ K, where m_p is the mass of proton and *k* is the Boltzmann constant.[1]

KS99 imposed a random artificial torque in the photosphere throughout the calculation. The function *L*(t,s) is chosen as

[1] For simplicity, Kudoh & Shibata assumed that the fluid consists of only hydrogenIf the mean molecular weight is not equal to unity, the temperature is changed from the value used in this paper.

L (r, s) = 2r [rand (t) - 0.5] f x {tanh [(z - 0.75 H_0)/(0.075 H_0)] - 1}, (20)

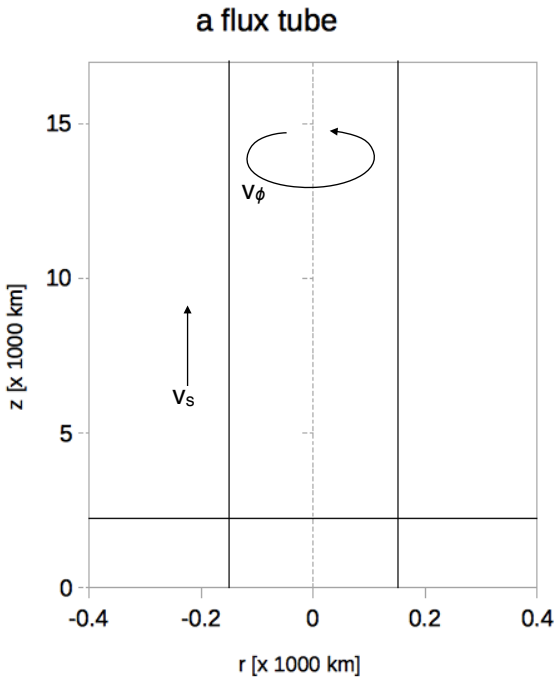

Fig 1. Initial shape of the magnetic flux tube from the photosphere. The transition region is initially z = 2250 km from the photosphere.

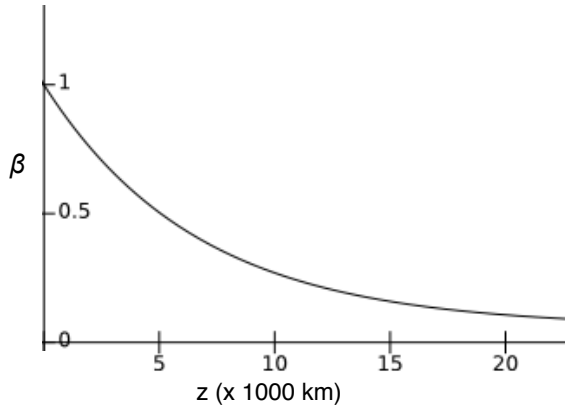

Fig 2. Initial plasma β (=8πP/B_s^2) as a function of height

where rand(t) is a random value between 0 and 1, which varies with time, and f is the parameter that determines the strength of the torque. The random perturbation in the photosphere is an assumption.

The grid size is chosen to be $\Delta s = 0.04\ H_0$ below z = 30 H_0 and it increases as $\Delta s_{i+1} = 1.02\ \Delta s_i$ until $\Delta s_i = 50\ \Delta s$. The total number of grids is 1024. The gravitational acceleration is chosen to be g = 0 above z = 400 for numerical convenience.

The simulation software package used in this research is CANS[2]. The numerical computational scheme used is the Modified Lax-Wendroff scheme.

A rigid wall boundary condition is implemented at z = 0 and a free boundary condition at the top of the computing region (at z ~ 286 H_0). Figures 3 shows the variation of log ρ and temperature along height from photosphere at time = 0 t_0. The chromosphere expands and adiabatically cools to very low temperature (Hollweg et al. 1982). The initial transition region height is 15 H_0. At the photosphere, z = 0 H_0, a rigid wall boundary condition is implemented such that the velocity is 0 km s^{-1} at z = 0 H_0.

3.2 The Modified Model

In order to study the effects of the convection zone, the computational region is extended underneath the photosphere. Figure 4 shows the variation of log ρ and log temperature along distance from photosphere at time = 0 t_0. Below z = 0 H_0 is the convection zone. The photosphere is at z = 0 H_0. The chromosphere expands and adiabatically cools to very low temperature (Hollweg et al. 1982). The initial transition region height is 15 H_0. At z = -20 H_0, a rigid wall boundary condition is implemented such that velocity = 0 km s^{-1} at z = -20 H_0. The density, pressure and temperature functions are solved by assuming adiabatic energy. See Table 1 for a summary of the initial set ups for the reproduction of KS99 and the modified KS99.

Case	Location of lower boundary	Location of transition region	Note
A	s = 0 H_0	s = 15 H_0	Reproduction of KS99
B	s = -20 H_0	s = 15 H_0	Modified KS99 model

Table 1. Summary of the two cases with different lower boundary locations and identical transition region location, where H_0 = 150 km.

[2] MHD simulation software package: CANS (Coordinated Astronomical Numerical Software).

4. RESULTS

Case A: Reproduction of KS99

The parameter *f*, which determines the strength of torque, in the artificial torque equation was set to be 1.03. Figure 5 shows the time variation of log ρ along the flux tube. The plots at various times are stacked with time increasing upward in uniform increments of 2.5 t_0. The transition region is lifted up and falls down, showing ballistic motions. The simulations agree with KS99's results. At a torque strength of 1.03, the maximum height of the transition region is about 5300 km from the photosphere and the initial perturbation velocity r.m.s. at the photosphere is about 0.4 km s^{-1}. Although the upward motions of the chromospheric materials are decelerated by gravity and eventually fall, energy is constantly being inputted in the photosphere under the assumption of adiabatic gas and therefore the transition region gradually gets higher and higher. Including some cooling effects, such as radiative cooling, would let the transition region falls back to its original location. Figures 6 shows the time variation of v_s and v_ϕ. Figures 7 shows the same plots for v_s and v_ϕ for t = 0-14 t_0. It can be clearly seen that transverse motions (in ϕ direction) generate longitudinal motion (in s direction) through nonlinear coupling. The longitudinal motion propagates as a slow wave slower than the Alfvén waves (β < 1). As the density decreases in the upper chromosphere, the slow wave is amplified to be a shock and eventually lifts the transition region up.

Case B: The Modified Model

The parameter *f* in the artificial torque equation was set to be equal to 1.03. Figure 8 shows the time variation of log ρ along the flux tube. The plots at various times are stacked with time increasing upward in uniform increments of 2.5 t_0. The transition region is not lifted up, suggesting that this strength of torque is not sufficient to produce spicules. The initial perturbation velocity r.m.s. at the photosphere is 0.01 km s^{-1}. Figures 9 shows the time variation of v_s and v_ϕ. Wave motions exhibit in both s and ϕ direction, but the motion is too small to produce shocks.

The parameter, f, was then changed to 90. Figure 10 shows the simulation at this torque strength. The maximum height observed is about 5300 km and the initial perturbation velocity r.m.s. at the photosphere is about 0.6 km s^{-1}. Spicules are formed at this torque strength. Figures 11 shows the time variation of v_s and v_ϕ.

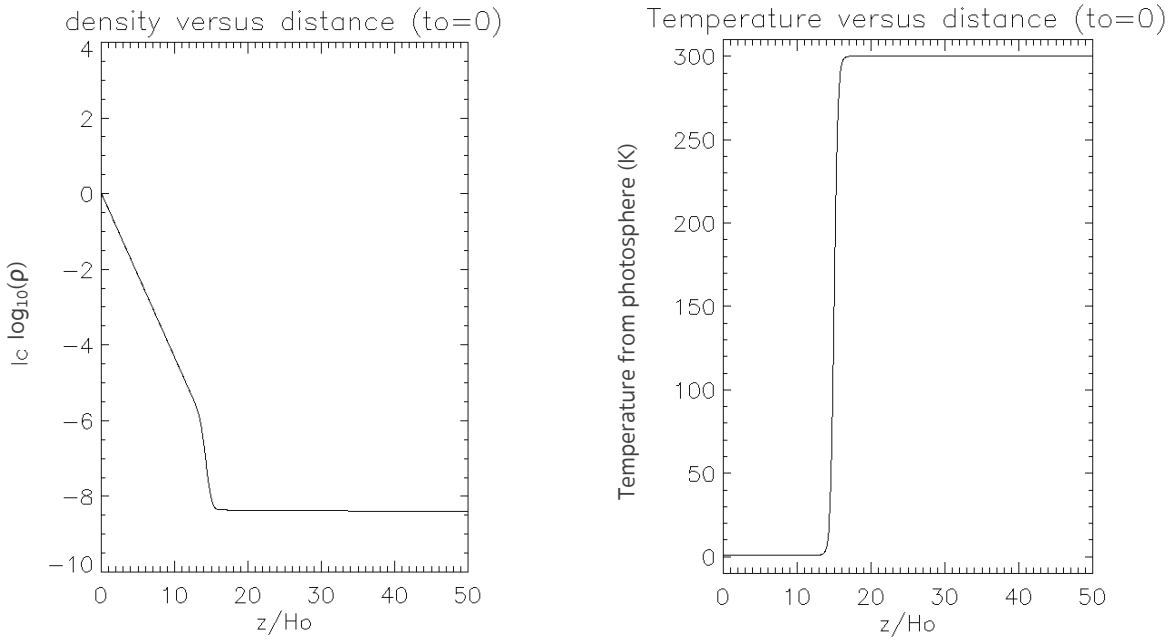

Fig 3. Initial setup of recreation of Kudoh & Shibata's model. Log density and temperature variation with height, where H_0 = 150 km and t_0 = 1.25 min. The photosphere is at z = 0 H_0. The initial transition region height is 15 H_0.

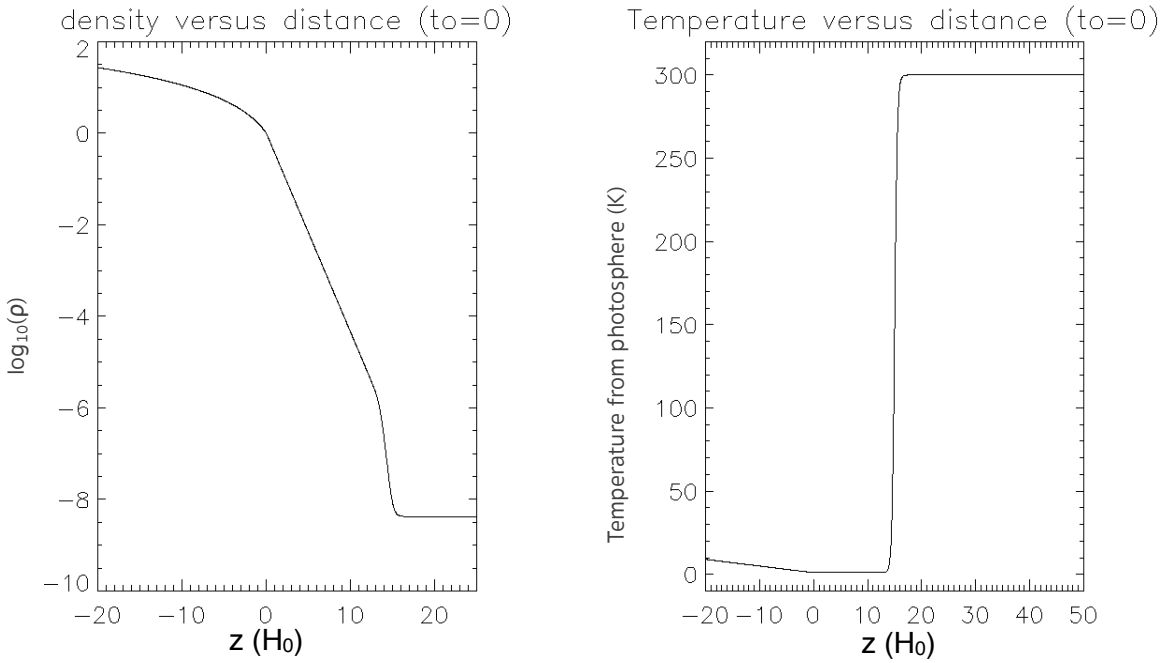

Fig 4. Initial set up of the modified model. Log density and temperature variation with height, where H_0 = 150 km and t_0 = 1.25 min. Below z = 0 H_0 is the convection zone. The photosphere is at z = 0 H_0. The initial transition region height is 15 H_0.

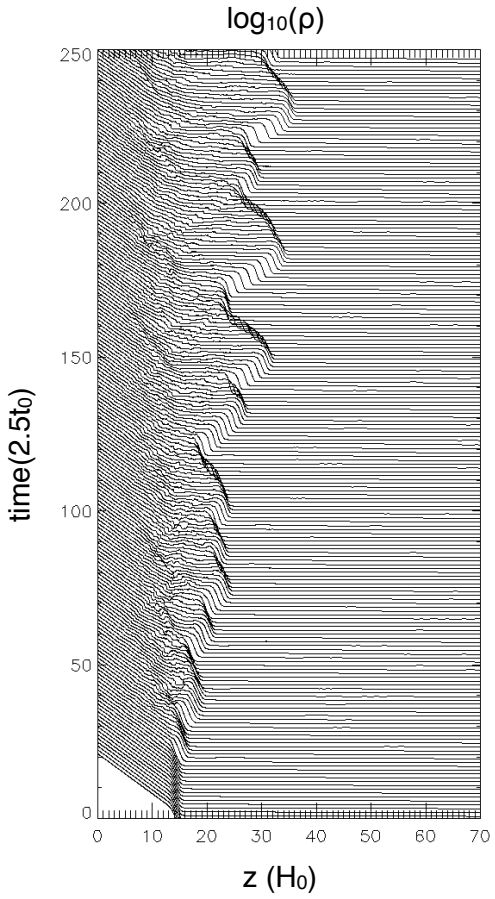

Fig 5. Time variation of density distribution, where H_0 = 150 km and t_0 = 1.25 min. The plots at various time are stacked with time increasing upward in uniform increments of 2.5 t_0.

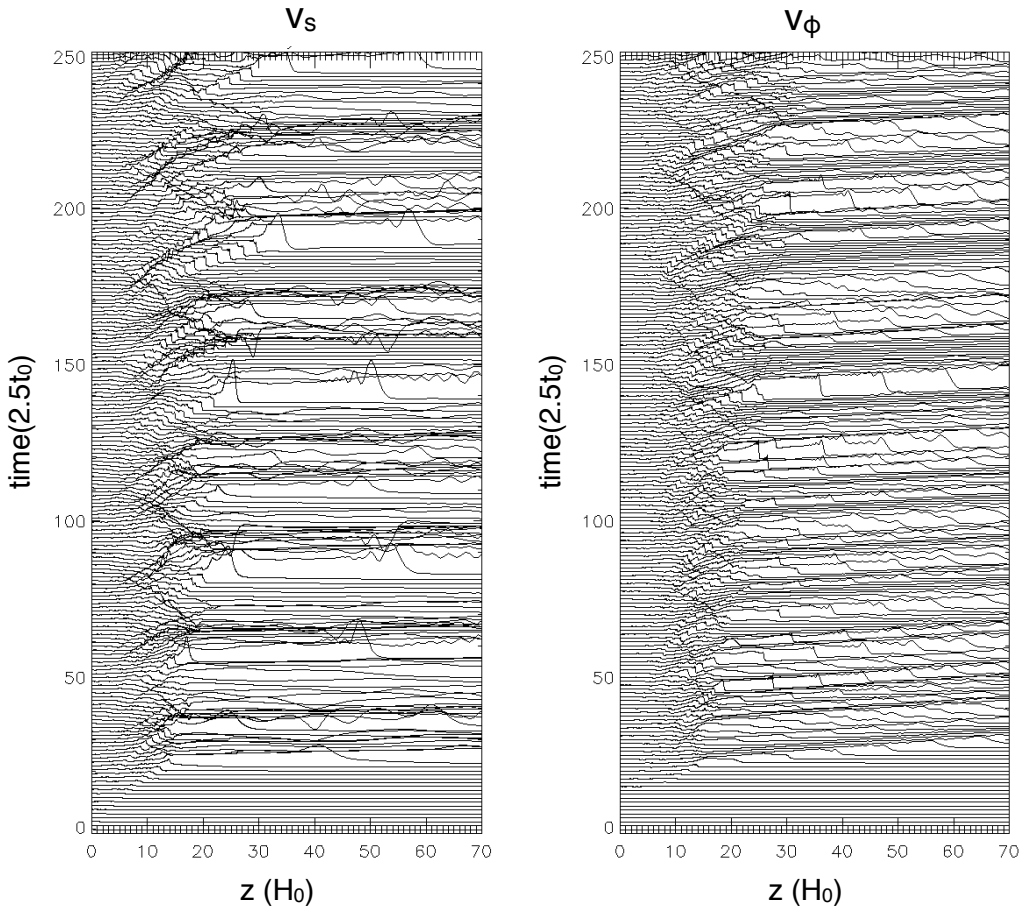

Fig 6. Time variation of v_s (left) and v_ϕ (right), where H_0 = 150 km and t_0 = 1.25 min. The plots at various time are stacked with time increasing upward in uniform increments of 2.5 t_0.

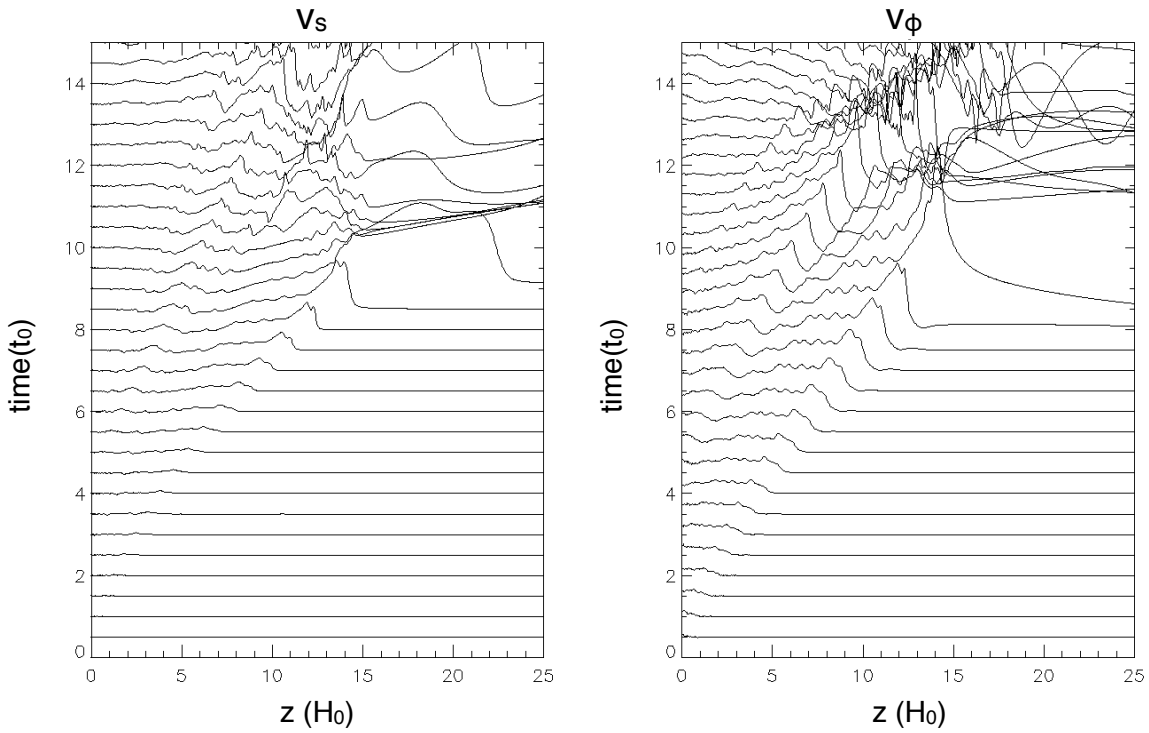

Fig 7. Time variation of v_s (left) and v_ϕ (right) for t_0 = 0 to 14, where H_0 = 150 km and t_0 = 1.25 min.

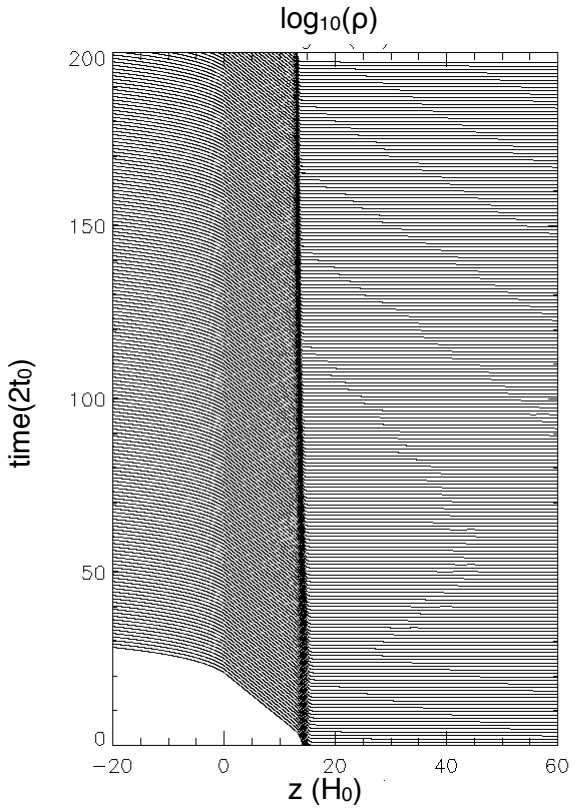

Fig 8. Time variation of density distribution, where H_0 = 150 km and t_0 = 1.25 min. The plots at various time are stacked with time increasing upward in uniform increments of 2.5 t_0.

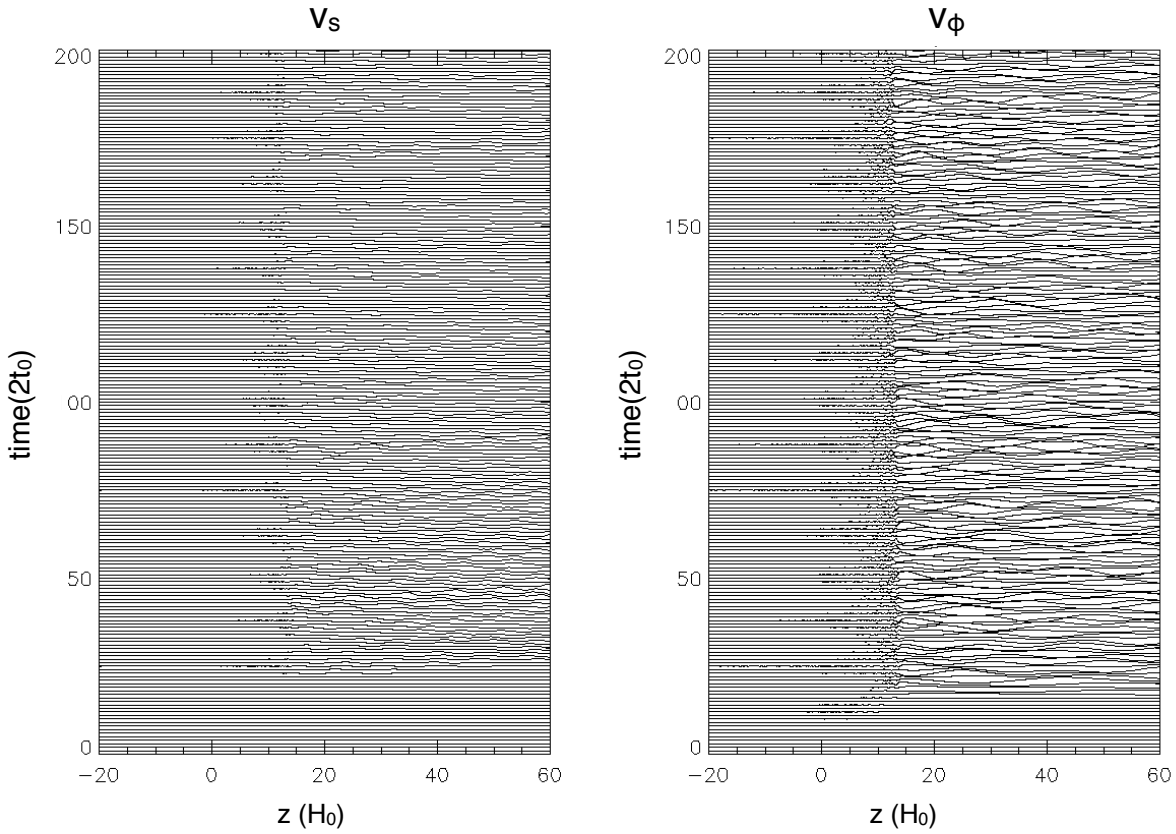

Fig 9. Time variation of v_s (left) and v_ϕ (right), where H_0 = 150 km and t_0 = 1.25 min. The plots at various time are stacked with time increasing upward in uniform increments of 2.5 t_0.

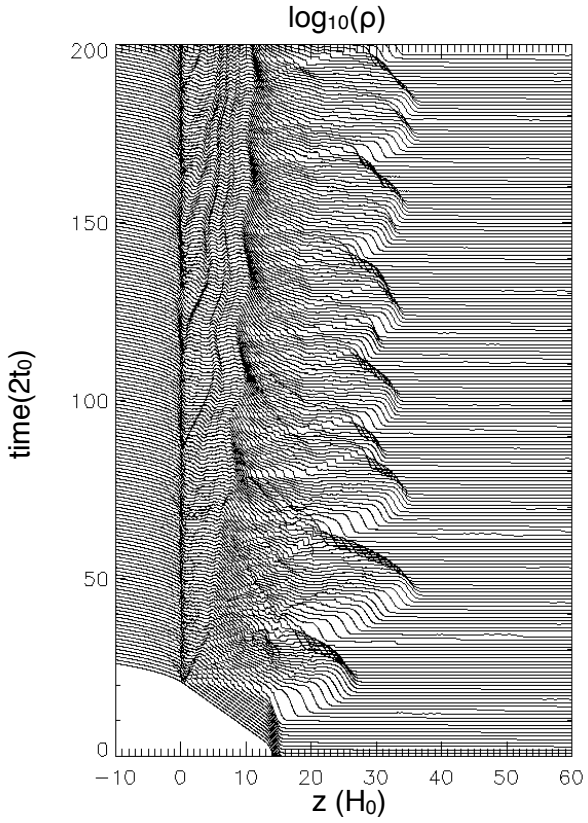

Fig 10. Time variation of density distribution, where H_0 = 150 km and t_0 = 1.25 min. The plots at various time are stacked with time increasing upward in uniform increments of 2 t_0.

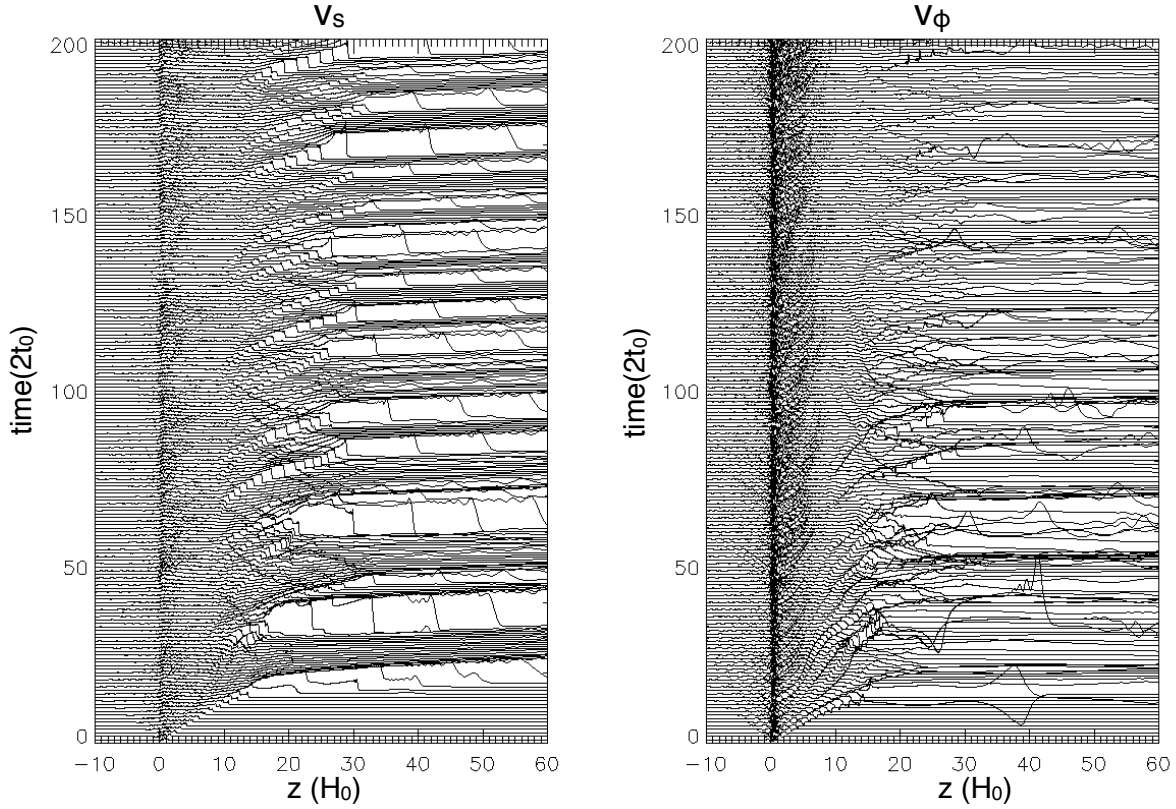

Fig 11. Time variation of v_s (left) and v_ϕ (right), where H_0 = 150 km and t_0 = 1.25 min. The plots at various time are stacked with time increasing upward in uniform increments of 2 t_0.

5. DISCUSSION

The main difference between our calculations and those of KS99 is the boundary condition in the photosphere. KS99 imposed a rigid wall boundary at z = 0 km, while we proposed that the continuous pressure gradient between the convection zone and the photosphere might have an effect on the input perturbations. Random perturbation was inputted throughout the calculation.

The spicule generation mechanism by MHD waves depends on the initial perturbations and plasma beta distribution in the chromosphere. The height of spicules also depends on the initial perturbations at the photosphere. Figure 12 shows the maximum spicule height from the photosphere as a function of the root mean square of initial perturbation velocity at the photosphere. It shows that in both model, the same amount of input perturbations can generate spicules of similar height, thus, the strength of torque only affects the input perturbation velocities.

The input torque required to generate the same perturbation in the photosphere was a lot greater in the modified model than that of KS99's. One possible cause was the propagation of waves in both directions from the photosphere. Figure 13 shows the time variation of v_ϕ as a function of height (photosphere at z = 0 H_0) for torque strength = 15. Part of the energy is lost as it propagates into the convection zone, thus reducing the height of the spicule. The amount of energy propagated into the convection zone and chromosphere is shown as a function of time in figure 14. Red represents the kinetic energy propagating into the chromosphere and blue represents the kinetic energy propagating into the convection zone. The amount of energy propagated into the convection zone and chromosphere was expected to be roughly equal, but results show that it is much bigger within the convection zone. This propagation of energy is still under analysis.

In our model, we assumed ideal MHD and neglected other dissipation effects such as radiative cooling and thermal conduction. The radiative cooling should affect the dynamics of the spicules in the chromosphere by reducing the maximum height of the transition region. The simulations could also be improved with smaller grid sizes, which could increase the accuracy in computation. In this research, a 1.5-dimensional model is used. One future direction of this project is to run 2-dimensional or 3-dimensional simulations which could provide greater detail in the non-axisymmetric features around the magnetic flux tube.

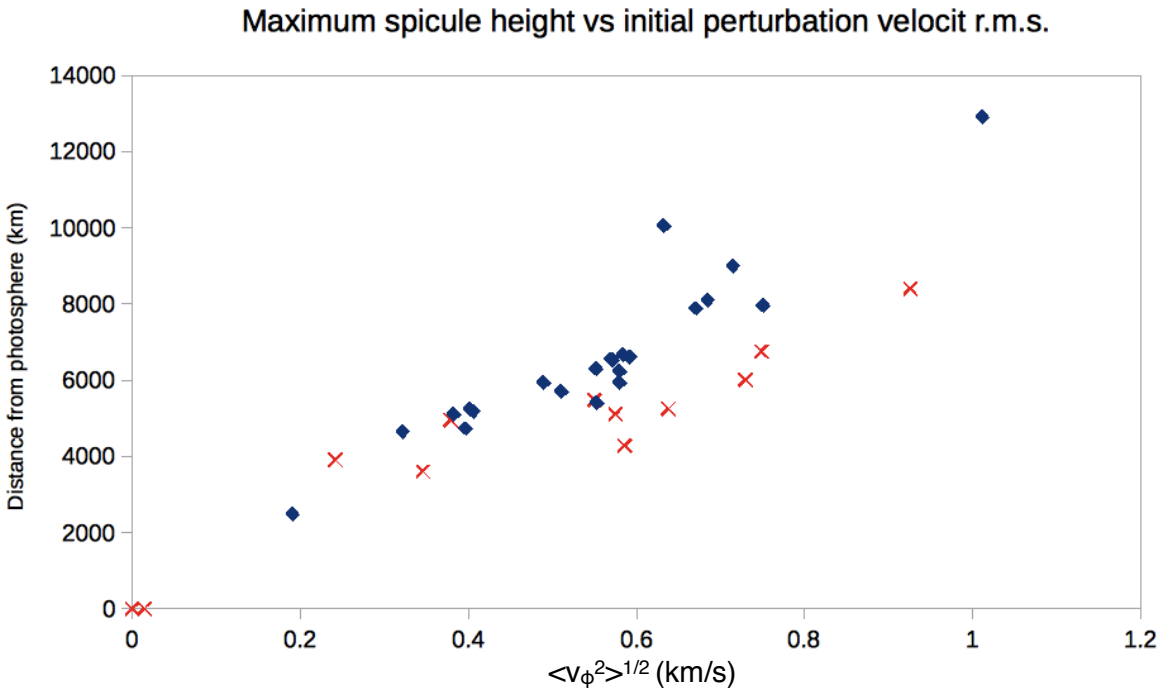

Fig 12. Maximum spicule height as a function of $<v_\phi^2>^{1/2}$ in the photosphere. Spicules heights from Kudoh & Shibata's model is plotted as blue diamonds (model1) and red crosses (model2) are that from the modified model.

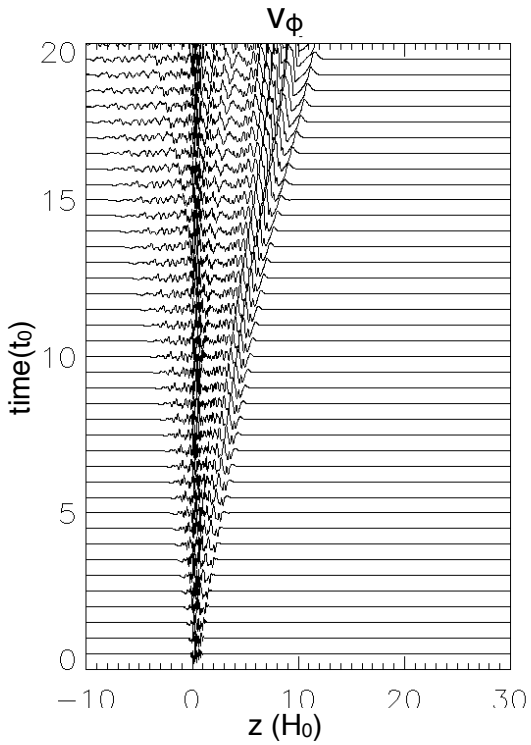

Fig 13. Time variation of v_ϕ at a torque strength of 15 from t = 0-20 t_0, where H_0 = 150 km and t_0 = 1.25 min.

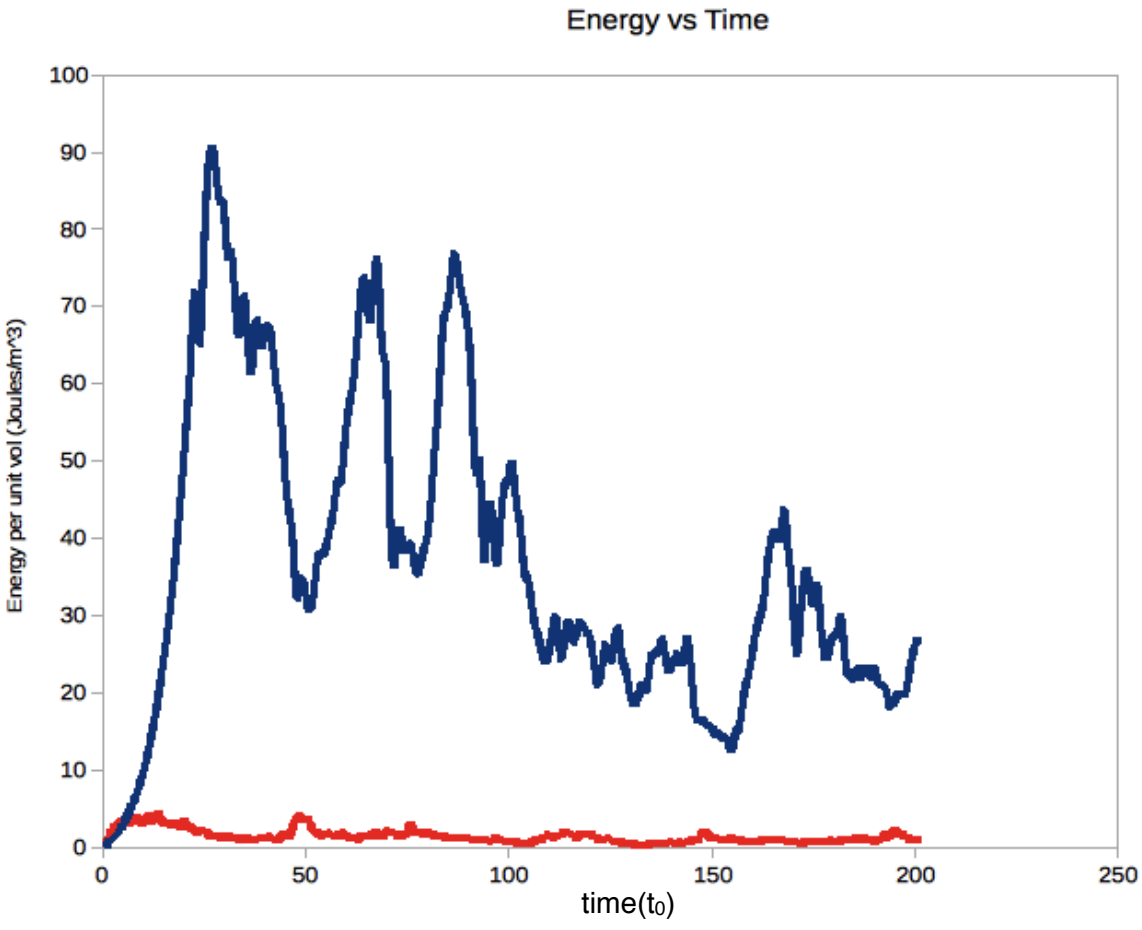

Fig 14. Energy as a function of time. Red represents the kinetic energy propagating into the chromosphere. Blue represents the kinetic energy propagating into the convection zone.

5. CONCLUSION

The 1.5-dimensional MHD simulations from KS99 was reproduced to study the spicule formation mechanism. Simulations suggest that Alfvén wave can be generated by random motions in the photosphere, which propagates upwards in the solar atmosphere and excited slow and fast shocks. As a result, the transition region is lifted up to more than ~ 5000 km and observed as spicules. The model was then modified to include the convection zone region for a more realistic model. Simulations show that spicule heights are reduced. The input artificial torque has to be increased by ~ 90 times greater than the original value in order to lift up the transition region to more than ~ 5000 km. The results show that boundary conditions near the photosphere could have an effect on the spicule height.

ACKNOWLEDGEMENTS

I would like to take this opportunity to express my gratitude to my supervisor, Prof. Takaaki YOKOYAMA for his guidance, wisdom and support he provided throughout this internship, and for welcoming me to his laboratory.

I would also like to thank my supporter, Mr. Y. Wang, and the Yokoyama Laboratory members, Mr. Y. Bekki, Mr. T. Kaneko, Mr. Y. Oi, Mr. C. Ichimura, Mr. S. Kono and Mr. M. Shoda for their help, advice and hospitality.

I had a wonderful research experience and learned a lot about Japanese cultures. I really appreciated this opportunity to work at the University of Tokyo and would like to thank the UTRIP staff for organising this research internship programme and all the support throughout this 6 weeks.

REFERENCES

Hollweg, J. V., Jackson, S., & Galloway, D. 1982, Solar Phys, 75, 35

Hollweg, J. V., 1992, ApJ, 389, 731

Hanayama, H., CANS manual, pp.18-35

Goedbloed, J. P., & Poedts, S. 2004, Principles of Magnetohydrodynamics: With Applications to Laboratory and Astrophysical Plasmas, Cambridge University Press, pp. 131-229

Kudoh, T., & Shibata, K. 1999, The Astrophysical Journal, 514:493-505